Environmental Science & Technology

Article

pubs.acs.org/est

Abiotic Reductive Immobilization of U(VI) by Biogenic Mackinawite

Harish Veeramani,*[,†] Andreas C. Scheinost,[‡] Niven Monsegue,[§] Nikolla P. Qafoku,[∥] Ravi Kukkadapu,[⊥] Matt Newville,[¶] Antonio Lanzirotti,[¶] Amy Pruden,[#] Mitsuhiro Murayama,[§,#] and Michael F. Hochella, Jr.[†,∥]

[†]Department of Geosciences, Virginia Tech, Blacksburg, Virginia, United States

[‡]Institute of Radiochemistry, FZD and Rossendorf Beamline, European Synchrotron Radiation Lab, Grenoble, France

[§]Department of Materials Science and Engineering, Virginia Tech, Blacksburg Virginia, United States

[∥]Geosciences Group, Pacific Northwest National Laboratory, Richland, Washington, United States

[⊥]Environmental Molecular Sciences Laboratory, Pacific Northwest National Laboratory, Richland, Washington, United States

[¶]Center for Advanced Radiation Sources, Advanced Photon Source (APS), Argonne, Illinois, United States

[#]Institute of Critical Technology and Applied Sciences, Virginia Tech, Blacksburg, Virginia, United States

Supporting Information

ABSTRACT: During subsurface bioremediation of uranium-contaminated sites, indigenous metal and sulfate-reducing bacteria may utilize a variety of electron acceptors, including ferric iron and sulfate that could lead to the formation of various biogenic minerals in situ. Sulfides, as well as structural and adsorbed Fe(II) associated with biogenic Fe(II)-sulfide phases, can potentially catalyze abiotic U(VI) reduction via direct electron transfer processes. In the present work, the propensity of biogenic mackinawite ($Fe_{1+x}S$, x = 0 to 0.11) to reduce U(VI) abiotically was investigated. The biogenic mackinawite produced by *Shewanella putrefaciens* strain CN32 was characterized by employing a suite of analytical techniques including TEM, SEM, XAS, and Mössbauer analyses. Nanoscale and bulk analyses (microscopic and spectroscopic techniques, respectively) of biogenic mackinawite after exposure to U(VI) indicate the formation of nanoparticulate UO_2. This study suggests the relevance of sulfide-bearing biogenic minerals in mediating abiotic U(VI) reduction, an alternative pathway in addition to direct enzymatic U(VI) reduction.

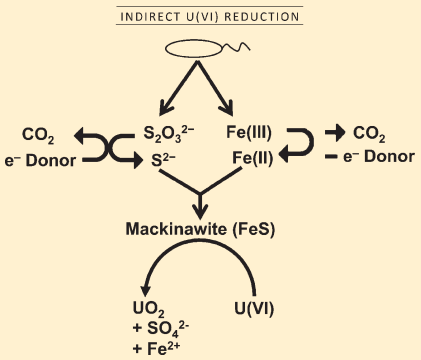

1. INTRODUCTION

Microbially mediated reduction of aqueous hexavalent uranium U(VI) to promote the formation of the sparingly soluble mineral uraninite [UO_2] represents a promising strategy for the in situ immobilization of uranium in subsurface sediments and groundwater at contaminated sites. In compositionally heterogeneous subsurface environments such as sediments, indigenous microbes including dissimilatory metal reducing (DMRB) and dissimilatory sulfate reducing (DSRB) bacteria can encounter multiple electron acceptors including Fe(III), Mn(IV), sulfate, and nitrate. Although the utilization of terminal electron acceptors is often assumed to be sequential from the highest to the lowest energy yield,[1] iron and sulfate reduction have been observed to occur either concurrently or sequentially in several field studies.[2−5] While preferential or competitive terminal electron accepting processes reported in most laboratory studies do not necessarily represent natural events in the subsurface, their potential occurrences cannot be excluded during biostimulation trials for uranium remediation.[6] Due to the abundance of Fe(III) in the subsurface,[7−9] the biostimulation of DMRB will likely lead to biological Fe(III) reduction[3,10,11] resulting in the formation of aqueous ferrous iron [Fe^{2+}], sorbed Fe(II) species,[12] and the formation of secondary mineralization products in situ including reactive Fe(II)-bearing biogenic minerals.[13−23] Biogenic Fe(II)-bearing minerals can provide a reservoir of reducing capacity where reduction of U(VI) may occur due to abiotic interactions[17,22] and potentially compete with direct enzymatic reduction[24] of U(VI). Abiotic U(VI) reduction is a thermodynamically favorable but often kinetically limited process and has been reported to be mediated by adsorbed Fe(II) species,[23−31] structural Fe(II) present in Fe(II)-bearing[17,22,32−34] and ferrous-sulfide bearing minerals such as pyrite (FeS_2),[35−37] mackinawite ($Fe_{1+x}S$),[38−40] and amorphous iron-sulfide.[41] Mackinawite is an environmentally relevant biogenic mineral[42] and is the initial ferrous sulfide solid phase that forms under sulfate reducing conditions, both in column[42−44] and field-scale studies.[45] It plays a critical role in serving as a precursor to the formation of most other stable iron sulfide phases[46,47] among

Received: October 3, 2012
Revised: January 27, 2013
Accepted: February 4, 2013
Published: February 4, 2013

which pyrite (FeS_2) is the most abundant.[48] It may also immobilize pollutant metals such as chromium[49] and selenium[50] through abiotic reduction, thus playing an important role in the remediation of contaminated sites.

Studies investigating abiotic interactions between synthetic mackinawite or amorphous iron sulfide and hexavalent uranium have reported considerable variations in their findings ranging from evidence of complete uranium reduction[38] to the formation of a mixed-valence U(IV)−U(VI) phase.[39−41] While the reactivity of synthetic iron sulfides has been researched extensively, the reactivity of biogenic mackinawite toward uranium remains largely unknown. Biogenic mackinawite formed under biostimulated conditions has been shown to act as an effective redox buffer by delaying the oxidative dissolution of UO_2.[42] It is therefore apparent that understanding the reductive immobilization of uranium in the presence of biogenic mackinawite is necessary due to its potential relevance and implications for long-term U(IV)/UO_2 reactivity. This is the first study to demonstrate the propensity of biogenic mackinawite to reduce aqueous uranyl species to nanoparticulate UO_2 by a combination of wet chemistry analyses, X-ray absorption spectroscopy (XAS), and transmission electron microscopy (TEM).

2. MATERIALS AND METHODS

2.1. Solutions. Unless indicated otherwise, sample preparation, experimental setup, and subsequent experimental procedures were conducted under strict anoxic conditions—either in serum bottles equipped with a butyl rubber septum and an aluminum crimp or inside an anoxic chamber with an atmosphere of 2.2% H_2 and 97.8% N_2. All chemicals used were of ultrapure analytical grade. Stock solutions were boiled and purged for several hours with N_2 before use. Glassware was soaked in 10% HCl overnight (ca. 14 h) and washed 5 times with deionized water and Milli-Q water, respectively, prior to use. A sterile solution of U(VI) was prepared by dissolving uranyl acetate powder (Ted Pella) in Milli-Q water (20 mM) and filter-sterilized using a syringe filter (0.2 μm polyethersulfone (PES)). The uranyl acetate solution was stored in an amber colored bottle inside an anoxic chamber.

2.2. Biogenic Mackinawite Synthesis. A culture of *Shewanella putrefaciens* CN32 was cultured in a minimal medium (M4 medium). The composition and culturing conditions are described in the Supporting Information (SI). For biogenic mackinawite synthesis the active culture was inoculated into sterile M4 medium (in an anoxic bottle) containing Fe(III)-citrate (50 mM), sodium thiosulfate (25 mM), and lactate (50 mM). The culture was incubated on a rotary shaker (140 rpm) at 28 °C (New Brunswick Scientific 12500). At timed intervals, 0.5 mL of sample from the anoxic bottle was withdrawn using a sterile syringe and needle (prepurged with sterile N_2) and acidified using 0.5 mL of 1 M HC. Fe^{2+} in the HCl extract was measured within 2 weeks by the ferrozine colorimetric assay as described by Stookey[51] using a spectrophotometer (Beckman Coulter DU 640 UV−vis). The loss of thiosulfate from solution was not measured during biogenic mackinawite synthesis.

2.3. Characterization of Biogenic Mackinawite. After observing steady-state Fe^{2+} concentrations, the anoxic bottles containing the biogenic mackinawite were allowed to stand static inside an anoxic chamber (COY Laboratory Products, Inc., Grass Lake, MI) for a week to allow for settling of the mineral. The supernatant was decanted and the precipitate was resuspended in 100 mL of anoxic Milli-Q water and transferred into gastight centrifuge bottles equipped with an O-ring. The bottles were centrifuged at 10 000*g* for 10 min. This washing procedure was repeated five times. All sample manipulations were carried out under stringent anoxic conditions.

2.3.1. X-ray Powder Diffraction (XRD). A detailed description of the sample preparation and instrumental analysis is provided in Section S2 of the SI. Qualitative analysis and mineral identification was done by using the PDXL: Integrated X-ray powder diffraction software.[52]

2.3.2. Electron Microscopy (EM). Samples for scanning electron microscopy (SEM) were prepared inside an anoxic chamber by loading washed and diluted sample on a carbon-coated grid (Ted Pella 01840) that was placed on a 12-mm double-coated carbon conductive tab (Electron Microscopy Sciences 77827-12) which in turn was mounted on a standard aluminum stub. Samples for SEM were analyzed using a LEO 1550 equipped with a secondary electron in-lens detector. The electron beam energy was set to 5 KeV and images were acquired using the secondary electron mode. The specimens for transmission electron microscopy (TEM) examination were also prepared by loading dilute samples on double-layer carbon-coated copper grids (Pacific Grid-Tech Cu-300HD) and allowed to dry inside an anoxic chamber. The FEI TITAN 300 TEM used in this study was operated at 300 kV (HRTEM) and equipped with an X-ray energy dispersive spectroscopy (EDS) chemical analysis unit (EDAX r-TEM) and a Gatan Orius SC200D CCD camera. Low dose illumination conditions were used to record the images in order to prevent beam-damage of particles under the electron beam. Crystalline phase identification was obtained by analyzing selected area electron diffraction (SAED) patterns and fast Fourier transforms of HRTEM images. The interpretation of HRTEM images, SAED patterns, and diffractograms were performed according to methods described elsewhere.[22] Electron diffraction patterns were indexed by comparing them with *d*-spacing values for mackinawite. An accuracy of ca. 5% was used.

2.3.3. Mössbauer Spectroscopy. A sample for Mössbauer spectroscopy measurement was prepared inside an anoxic chamber by filtering the mackinawite suspension through a 0.45-μm pore-size filter (Millipore Durapore Membrane Filter). Details of the sample preparation, Mössbauer spectrometer instrumentation, and modeling of the spectra are similar to that described elsewhere.[53] In brief, WissEl (Germany) Mössbauer electronics, and a closed-cycle cryostat SHI-850 and Sumitomo CKW-21 He compressor unit, obtained from Janis Research Company, Inc. (Wilmington, MA), were employed for the measurements. The Mössbauer data was modeled by the Recoil software (University of Ottawa, Canada) using a Voigt-based structural fitting routine.[54]

2.3.4. X-ray Photoelectron Spectroscopy (XPS). Details of the sample preparation and XPS analysis are provided in Section S3 of the SI.

2.4. Batch Abiotic uranium reduction. Batch U(VI) reduction experiments were carried out in sterile screw-cap polyethylene tubes inside a glovebox. An aliquot of the washed mackinawite suspension was added to tubes containing 50 mL of anoxic Milli-Q water yielding a final mass of 219.75 mg and a solid-to-solution ratio of 4.39 g/L. The resulting suspension was amended with 20 mM (final concentration) anoxic PIPES buffer set to pH 7 (Sigma P6757) and the pH was monitored several times during the experiment. The suspension was also amended with sodium bicarbonate to a final concentration of 1

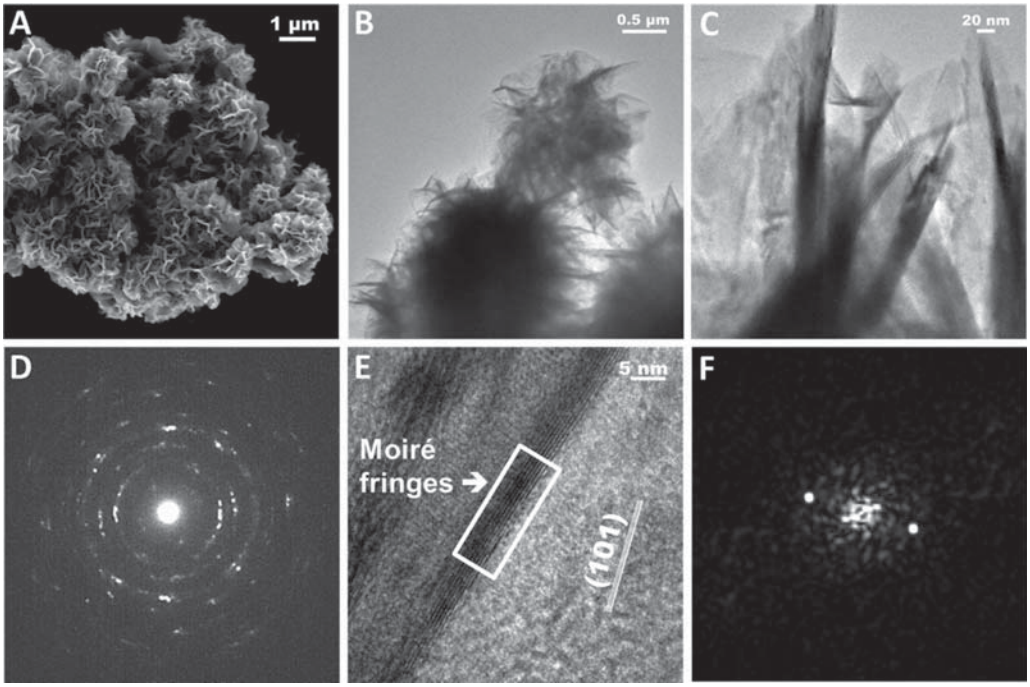

Figure 1. (A) SEM image; (B and C) TEM bright field image, (D) SAED pattern taken from an area biogenic mackinawite that is shown in 1C, and (E) HRTEM image of biogenic mackinawite. HRTEM shows Moiré fringes at a fold and a set of (101) lattice fringes confirmed by (F) fast Fourier transform from the region.

mM. To rule out potential enzymatic uranium reduction by CN32, an aliquot of biogenic mackinawite was pasteurized by heating it at 80 °C for 20 min. This pasteurized biogenic mackinawite was used as a control in a parallel U(VI) reduction experiment. Uranium reduction was initiated by amending a solution of uranyl acetate to suspensions of biogenic mackinawite (unpasteurized and pasteurized) yielding a final U(VI) concentration of 0.001 M. At timed intervals, two aliquots (0.5 mL each) were withdrawn to measure uranium concentration. One of the samples was filtered through a 10-mm syringe filter (0.02-μm Whatman 6809-1102 Anotop 10). The filtrate was diluted in 0.1 M HNO_3 and analyzed for total dissolved uranium using inductively coupled plasma atomic emission spectroscopy (ICP-AES) (Spectro ARCOS SOP - Spectro Analytical Instruments, Inc.). This measurement targeted the disappearance of uranyl species from solution. The second sample was treated with an anoxic solution of 0.1 M bicarbonate (final concentration), stored at 25 °C overnight, filtered through a 0.02-μm pore size filter, and analyzed using the ICP-AES as above. The detection limit of the ICP-AES was 0.126 ppm. The bicarbonate treatment procedure enabled preferential desorption of U(VI) species from the mineral surface (due to formation of uranyl carbonate complexes) and the analysis of the bicarbonate extract revealed the amount of adsorbed uranyl species. Samples were withdrawn, treated, and filtered under strict anoxic conditions to prevent oxidation of U(IV). The amount of U(VI) reduced could be calculated by subtracting the amount of U(VI) recovered from the total amount of uranium associated with the solid phase.

2.5. X-ray Absorption Spectroscopy (XAS). Following U(VI) reduction, the biogenic mackinawite suspensions were centrifuged at 10 000*g*. The resultant wet pellets were filled into individual Plexi-glass sample holders equipped with Kapton windows. The sample holders were shipped to the Advanced Photon Source (APS) in a gastight container for XAS analysis. XAS analysis included X-ray absorption near edge structure (XANES) and extended X-ray absorption fine structure (EXAFS). All sample manipulation and handling at the beamline was performed under an argon flux. U L_{III}-edge transmission spectra were collected at room temperature conditions at the GSECARS−University of Chicago 13-BMD beamline, using a Si(111) low energy monochromator and 16-element HPGe array detector (Canberra). Energy calibration was carried out using an yttrium foil prior to measurements. Vertical beam height on the monochromator crystal defines the energy resolution to be smaller than the intrinsic U L_{III}-edge line width. EXAFS spectra were background subtracted, splined, and analyzed using the WinXAS program.[55]

3. RESULTS AND DISCUSSION

3.1. Biogenic Mackinawite Synthesis. Iron reduction was observed in the *S. putrefaciens* CN32 culture as indicated by the production of Fe(II) over the course of incubation (Figure SI-1). The concentration of Fe(II) was found to be constant after 90 h indicating iron reduction had reached its capacity (Figure SI-1). The bioreduction of Fe(III)-citrate and thiosulfate by *S. putrefaciens* CN32 resulted in the formation of a black precipitate, which settled over a 4-d stagnant period.

3.2. Biogenic Mackinawite Characterization. *3.2.1. XRD.* Qualitative background-subtracted powder diffraction analysis of the washed biogenic mineral (Figure SI-2) confirmed the formation of crystalline mackinawite with no other phases apparent in the XRD pattern. The XRD Bragg reflection peaks of the sample exhibited peak broadening due to the small crystallite size. The biogenic mackinawite was highly reactive and oxidized rapidly to form lepidocrocite (γ-FeOOH) upon extended exposure to air. It is important to note that the sample was pure and devoid of other mineral phases as

confirmed by additional analyses described below. Pyrite precursors such as mackinawite and greigite (Fe_3S_4) are typically sensitive to oxidation, which makes their characterization by conventional powder X-ray diffraction (XRD) difficult.[56] However, enclosing the sample between two layers of Kapton tape dramatically slowed the oxidation process, thus permitting reliable and consistent diffraction measurements.

3.2.2. Electron Microscopy. Scanning electron microscopy revealed aggregates of biogenic mackinawite composed of a large number of rosette-like particles. Transmission electron microscopy further revealed the intricate details within the micrometer sized rosette-like assemblages (Figure 1A and B). The morphology of the biogenic mackinawite aggregates seemed unaffected by the pasteurization process as observed by SEM (Figure SI-3). Higher magnification of the rosette-like assemblages showed that they were made up of thin films arranged in an irregular yet unique morphology (Figure 1C). The morphology of the rosette-like biogenic mackinawite assemblages produced by *Shewanella putrefaciens* CN32 is similar to the biogenic mackinawite produced by sulfate-reducing bacteria[57] and markedly different from that of synthetic mackinawite that varies in shape and morphology ranging from irregular shaped single crystals[58] to flake-like nanoparticles[59] and overlapping layered particles.[60] Energy dispersive X-ray spectroscopy (EDS) analysis on the selected area of the biogenic mineral indicated that it is composed of Fe and S (Figure SI-4). SAED obtained from the FeS aggregates displayed ring patterns (Figure 1D) with *d*-spacings that match mackinawite. HRTEM examination of the biogenic FeS aggregates showed that they consist of irregularly aggregated, thin film-like crystals (Figure 1E). The HRTEM image reveals a set of lattice fringes corresponding to (101) planes of mackinawite that is also confirmed by measuring their *d*-spacing using fast Fourier transform of the corresponding HRTEM image region (Figure 1F). Moiré fringes are observed at a fold due to overlapping crystals of the FeS film sheets (Figure 1E).

3.2.3. Mössbauer Analysis. Mössbauer spectroscopic measurements at room, liquid nitrogen (77 K; not shown), and near liquid He (4.2 K) temperatures were obtained to investigate oxidation and coordination states of Fe environments, as well as purity of the synthetic mackinawite. At all temperatures, the spectral features show a characteristic singlet due to low spin Fe(II) in the tetrahedral environment (Figure SI-5). The derived RT Mössbauer spectral parameters of the singlet (center shift = 0.38 mm/sec and quadrupole shift = 0.2 mm/sec) are in agreement with numerous studies on mackinawite[58] (Figure 2). More or less similar spectral features of RT and liquid He spectra (Figure 2), without any sextet contribution, indicate the absence of Fe(III)-bearing phases.[61]

3.2.4. XPS. The XPS survey scan of the biogenic mackinawite indicated the presence of O, C, S, and Fe at the sample surface (Figure SI-6). Eliminating oxygen at the sample surface was not possible despite the precautions taken during sample preparation. The broad Fe($2p_{3/2}$) peak in the HR-XPS spectra (Figure SI-7) near 707 eV corresponds to the binding energy of Fe(II)-S compounds.[58,62,63] The S($2p_{3/2}$) peak at 161.3 eV (Figure SI-7) is typically attributed to monosulfide species[58] and has been reported by Herbert and co-workers[57] for biogenic mackinawite synthesized by sulfate-reducing bacteria.

3.3. Batch Abiotic Uranium Reduction. U(VI) amended to suspensions of biogenic mackinawite was removed from solution (below detection limits) within 5 min indicating rapid sorption (data not shown). Similar studies involving chemogenic iron sulfide have also reported rapid sorption of uranium over a wider range of pH values.[38,41] To determine the extent of mineral-associated U(VI) reduction, samples from the suspension were treated with a solution of anoxic bicarbonate (100 mM) which extracts the surface associated U(VI) but not U(IV) as mentioned above. A similar extraction method has been reported in a recent study involving abiotic reduction of uranium by biogenic vivianite.[22] Our results show that the concentration of surface-associated uranium was below detection limit within 120 h in the presence of biogenic mackinawite indicating complete reduction (Figure 2). The rate of U(VI) reduction in the pasteurized control was marginally faster than the unpasteurized control consistent with earlier studies involving pasteurized biogenic minerals.[22] The observed faster rate is presumably due to the liberation and sorption of Fe(II) from the biogenic FeS during pasteurization which can reduce U(VI) in addition to structural Fe(II) and S^{2-}. Overall, similar adsorption and reduction behavior is observed in the pasteurized and unpasteurized suspensions (Figure 2), suggesting an abiotic U(VI) reduction process. U(VI) reduction was not observed in the control lacking biogenic mackinawite. An anoxic bicarbonate treatment (1 M) which is known to extract monomeric U(IV) species from minerals and biomass[64] extracted less than 5% of the total uranium from the biogenic mackinawite (after uranium reduction) indicating that the reduced uranium was predominantly UO_2 and not monomeric U(IV) species (data not shown).

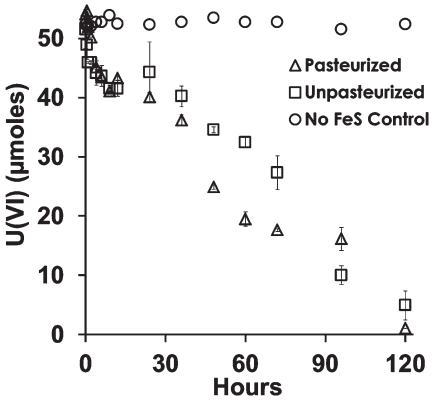

Sample	K_{obs} (h^{-1})	half-life (h)	r^2
Unpasteurized	0.0128	54.15	0.97
Pasteurized	0.0382	18.14	0.96

Figure 2. U(VI) reduction by unpasteurized (□) and pasteurized (Δ) biogenic mackinawite. Control (○) lacking biogenic FeS does not show U(VI) reduction.

3.4. Uranium Speciation. *3.4.1. Electron Microscopy.* HRTEM revealed the formation of UO_2 nanoparticles on the surface of biogenic mackinawite following uranium reduction (Figure 3A). This was also confirmed by elemental (EDS) analysis that revealed association of uranium with Fe and S (Figure SI-8). HRTEM of the biogenic mackinawite sample taken along the edge of the FeS film further confirmed the presence of crystalline nanoparticulate UO_2 with an approximate size of 2.5 nm (Figure 3B). SAED analysis on the nanoparticulate UO_2 yielded diffraction patterns that matched the reported *d*-spacing values for UO_2 (Figure 3C).

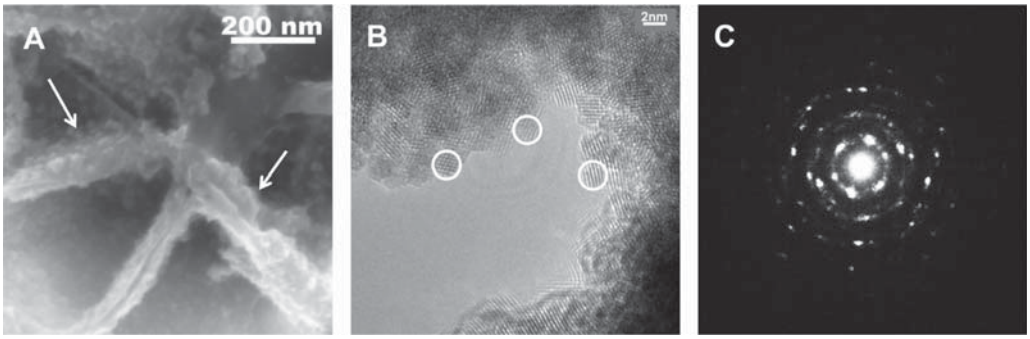

Figure 3. (A) Magnified SEM image showing UO_2 nanoparticles (indicated by arrows) on the surface of biogenic mackinawite; (B) UO_2 nanoparticles on the surface of biogenic mackinawite observed by HRTEM; (C) a corresponding nanodiffraction pattern confirming the presence of crystalline UO_2 phase.

3.4.2. X-ray Absorption Spectroscopy. XANES analyses of the pasteurized and unpasteurized biogenic mackinawite sample indicated the predominance of tetravalent uranium in that the energy of the absorption edge was identical to the UO_2 standard. The lack of a shoulder-like multiple scattering resonance feature after the absorption edge, considered indicative for uranyl species, suggests complete uranium reduction (Figure 4A). Uranium L_{III}-edge EXAFS, used to probe the molecular coordination environment of the reduced uranium phase, displayed a general spectroscopic signature for uraninite, most notably a U−O shell at 2.34 Å (Table 1) and a U−U shell at 3.83 Å (corresponding to the Fourier transform (FT) peaks at 1.8 and 3.8 Å, uncorrected for phase shift). The reduction in the amplitude of the chi spectra and increased Debye−Waller factor (limited to 0.0150 Å) is suggestive of higher structural disorder (biogenic mackinawite sample) as compared to the standard crystalline UO_2. The absence of the U−U backscattering contribution at 6.4 Å in the biogenic mackinawite samples (Figure 4C) is also suggestive of higher structural disorder and/or limited crystallite size. The FT peaks in the sample data for $R > 7$ Å are not observed due to the nanoparticulate size of uraninite (c.a. 2.5 nm). Furthermore, since the data were collected at room temperature, we cannot comment on the intermediate range structural order, but the short-range U−O (1.8 Å) and U−U (3.8 Å) peaks in the XAFS are characteristic of uraninite.

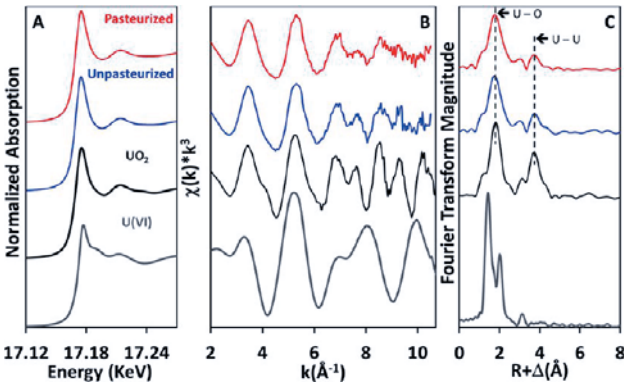

Figure 4. (A) XANES showing U(IV) in the presence of pasteurized and unpasteurized biogenic mackinawite. UO_2 and U(VI) reference spectra included for comparison; (B) U L_{III}-edge EXAFS spectra for UO_2 produced by pasteurized and unpasteurized biogenic mackinawite samples; (C) corresponding Fourier transforms. Fits listed in Table 1. The small FT peak at $R \approx 1.5$ Å ($R + dR$) is known to result from the presence of a multielectron excitation at $k = 10$. Two $Å^{-1}$ in all spectra.

Finally, differences in (1) the amplitudes of chi at the higher k-range, (2) FT amplitudes, and (3) the coordination numbers of next neighbor shells is suggestive of slightly less structural disorder of the UO_2 in the unpasteurized sample. These findings are generally consistent with previous studies involving abiotic U(VI) reduction.[17,22,38] Similar EXAFS results were observed for both unpasteurized and pasteurized biogenic mackinawite samples, agreeing with our hypothesis that an abiotic process leads to uraninite formation. A combination of TEM and XAS analysis thus confirms the formation of U(IV)/UO_2 at the bulk and nano scale, respectively.

3.5. Mechanism of U(VI) Reduction. XPS analysis on the biogenic mackinawite sample after U(VI) reduction indicated changes in the binding energy of S2p (Figure 5A). The signal-

Table 1. U L_{III}-Edge XANES Edge Energies and EXAFS Fit Results of Pasteurized and Unpasteurized Samples and References

	coordination shell			next neighbor shells				
sample	CN[a]	R^b [Å]	σ^{2c} [Å^2]	CN	R [Å]	σ^2 [Å^2]	DE_0 [eV]	X^2 res %
non pasteurized	8.0 O	2.34	0.0150[ul]	12.0 U	3.84	0.0150[ul]	2.2	15.9
				24.2 O	4.46	0.0150[ul]		
pasteurized	7.6 O	2.35	0.0150[ul]	10.0 U	3.83	0.0150[ul]	3.2	16.6
				17.9 O	4.43	0.0142		
crystalline UO_2	8.4 O	2.34	0.0133	10.1 U	3.85	0.0086	2.6	7.7
				20.5 O	4.46	0.0133		
XRD	8.0 O	2.37		12.0 U	3.87			
				24.0 O	4.54			

[a]CN = coordination number, error = ± 25%. [b]R = radial distance, error = ± 0.01 Å. [c]σ^2 = Debye−Waller factor, error (0.0005 Å^2).

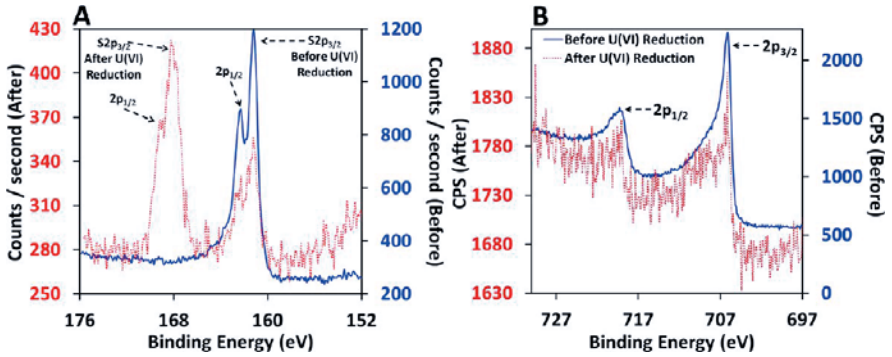

Figure 5. High resolution X-ray photoelectron spectroscopy (XPS) showing (A) the S2p binding energy, and (B) the Fe2p binding energy before and after U(VI) reduction. The counts per second (CPS) for the spectra before U(VI) reduction is shown on the primary *y*-axis. The CPS after U(VI) reduction is shown on the secondary *y*-axis. The decrease in counts is due to coating of the biogenic mackinawite surface with aggregates of nanoparticulate UO_2.

to-noise ratio was affected considerably due to the coating of the mackinawite surface with aggregates of nanoparticular UO_2 as seen in the SEM and TEM images (Figure 3). XPS analysis is a highly surface sensitive technique and the presence of even the thinnest coatings can affect the signal-to-noise ratio significantly for the surface elements that become covered. The S2p peak in the high resolution scan displays a noticeable shift in the binding energy from 161.2 to 168.3 eV (shift of 7.1 eV) after U(VI) reduction. The peak at 161.2 eV is indicative of residual and unreacted sulfide while the peak at 168.3 eV indicates the formation of sulfate which has been reported previously in studies involving the oxidation of sulfide-bearing minerals such as pyrrhotite[65,66] and pyrite.[67] Fits to the S2p peaks indicate the presence of approximately 67% sulfate and 33% sulfide on the surfaces of the biogenic mackinawite sample following U(VI) reduction (Figure SI-9). Sulfate was also recorded by ion chromatography in the samples of biogenic mackinawite (filtered 0.02 μm) after complete U(VI) reduction (data not shown). The binding energy for Fe(2p), however, remained unchanged (Figure 5B) after U(VI) reduction and is an indication of the inertness of Fe(II) in the present system contrary to other ferrous-bearing minerals such as biogenic magnetite[22] in which U(VI) reduction is driven by the structural ferrous ions. This finding is in agreement with Mössbauer spectroscopy that failed to identify ferric-bearing phases following U(VI) reduction (data not shown). Similar studies investigating abiotic interactions between U(VI) and amorphous FeS[41] and synthetic mackinawite[38] have suggested U(VI) reduction to occur by an ion exchange mechanism involving the release of Fe(II) to solution followed by the reduction of U(VI). Hua and co-workers[41] concluded that U(VI) reduction was driven by solid phase Fe(II) or HS− based on XPS and solution analysis but could not conclusively differentiate between the two mechanisms. Hyun and co-workers[38] reported the formation of elemental sulfur by coprecipitating UO_2 with synthetic mackinawite and inferred sulfides to be the electron provider. The present study differs from these earlier studies in two aspects: (1) the reduction of U(VI) is coupled to sulfide oxidation in which the structural sulfides are oxidized to form sulfate [SO_4^{2-}] ions as confirmed by XPS and ion chromatographic analysis; and (2) U(VI) was added to preformed and precharacterized biogenic mackinawite (not coprecipitated with FeS). The formation of sulfate has also been reported in studies involving Au(III) reduction on sulfide surfaces.[62,68] From equilibrium calculations (neglecting surface effects), the interaction between sulfide and uranium is predicted to involve the reduction of uranyl to crystalline UO_2 and the oxidation of sulfide to sulfate.[35,69,70] Although sorbed[27] and structural[22] Fe(II) is known to reduce U(VI), recent studies,[38,41] including the present work, involving iron sulfides demonstrate the reactivity of S^{2-} and inertness of Fe(II) toward U(VI) reduction. Interestingly, exposure of the biogenic mackinawite to air led to the formation of lepidocrocite (γ-FeO(OH)) (Figure SI-10) within a few minutes, indicative of rapid Fe(II) oxidation. These findings suggest the need to further investigate the role of sulfides in minerals such as mackinawite, pyrite, and marcasite which contain two reductants (S^{2-} and Fe(II)).

3.6. Environmental Implications. U(VI) reduction during in situ bioremediation is often thought to primarily occur via enzymatic reactions[71] driven by indigenous DMRB, which is the intent of biostimulation of uranium-contaminated sites. This study contributes to a growing body of evidence for abiotic processes mediated by biogenic minerals leading to the reductive immobilization of uranium.[17,22] Similar studies investigating the role of synthetic mackinawite and amorphous iron sulfide in uranium reduction have reported considerable variations in their findings ranging from evidence of complete uranium reduction[38] to the formation of a mixed-valence U(IV)−U(VI) phase.[39−41] Abiotic uranium reduction mediated by biogenic minerals such as mackinawite leading to the formation of UO_2 is one of the other important processes to consider when devising bioremediation schemes. U(VI) reduction may be indirectly driven in the subsurface by microbes via biogenic mackinawite that is produced as a secondary biomineralization product. Mackinawite is an environmentally relevant mineral and has often been reported to form during the biostimulation of sediments[42,72−74] as a result of biological reduction of Fe(III) and sulfate. Column studies simulating sulfate-reducing conditions that often occur during biostimulation have also demonstrated the formation of biogenic FeS in response to an electron donor amendment.[43,44] The formation of FeS in situ has been confirmed by electrical induced polarization measurements that were carried out at the Rifle Integrated Field Research Challenge (IFRC) site during a biostimulation experiment involving acetate amendments.[45] Its presence has also been confirmed by SEM and TEM analysis of biostimulated groundwater samples that revealed the presence of biogenic FeS and its association with bacterial cells.[45] It is a reactive mineral as demonstrated by its propensity to reduce

U(VI) in the present work and other redox active contaminants reported in related studies.[38,41,49,50] In addition, the formation of pyrite from iron monosulfide precursors in anoxic sediments have been suggested to proceed via mackinawite.[46,48] Pyrite is also capable of reducing U(VI) as reported by many laboratory studies.[35,36,75] Consequently, uranium is also found to be associated with framboidal pyrite in a naturally bioreduced alluvial sediment.[37] Given the precursory role of mackinawite in pyrite formation,[48,76] one potential explanation for the observed U−framboidal pyrite association in the field could be the gradual aging and transformation of mackinawite (containing reduced uranium) to framboidal pyrite. Furthermore, traces of mackinawite has been reported to coexist with framboidal pyrite[46] suggesting its participation in mediating U(VI) reduction even in the presence of pyrite. Mackinawite is also known to act as a redox buffer and render stability to the UO_2 in oxic environments.[42] UO_2 is sparingly soluble and thus the desired product of remediation.[38,77] By reconciling the findings reported in the present work and related studies, and knowing the relative ease of biogenic mackinawite formation and advantages of mackinawite in terms of its redox buffering capacity, alternative strategies could be developed for the remediation of uranium contaminated sites.

■ ASSOCIATED CONTENT

Ⓢ Supporting Information

Additional text and figures as mentioned in the text. This information is available free of charge via the Internet at http://pubs.acs.org/

■ AUTHOR INFORMATION

Corresponding Author

*Phone: +1-540-231-3058; e-mail: harish@vt.edu; mail: Dept. of Geosciences, 4044 Derring Hall, Virginia Tech, Blacksburg, VA 24060, USA.

Notes

The authors declare no competing financial interest.

■ ACKNOWLEDGMENTS

We thank Steve McCartney and Andrew Giordani at the NCFL (Nanoscale Characterization and Fabrication Laboratory), ICTAS, Virginia Tech for assistance with the electron microscope and XPS, respectively. We thank Biswarup Mukhopadhyay at Virginia Bioinformatics Institute (VBI) for provided access to a glove box and J. Donald Rimstidt at the Department of Geosciences, Virginia Tech for useful discussion. Funding for this project was provided by DOE-BER Grant DE-SC0006825 and DOE-BES Grant DE-FG02-06ER15786, and facilities were made available through the Virginia Tech's Institute for Critical Technology and Applied Sciences (ICTAS). Mössbauer analysis was performed at the Environmental Molecular Sciences Laboratory (EMSL) at PNNL under proposal 47291. We also thank Joanne Stubbs at CARS/University of Chicago for assistance at the APS/CARS beamline and Edward O'Loughlin at Argonne National Laboratory for advice in sample preparation for XRD analysis. A culture of *Shewanella putrefaciens* CN32 was provided courtesy of Colleen Hansel and Deric Learman (Harvard School of Engineering and Applied Sciences; now at Woods Hole Oceanographic Institute and Central Michigan University, respectively). Portions of this work were performed at GeoSoilEnviroCARS (Sector 13), Advanced Photon Source (APS), Argonne National Laboratory. GeoSoilEnviroCARS is supported by the National Science Foundation - Earth Sciences (EAR-1128799) and Department of Energy - Geosciences (DE-FG02-94ER14466). Use of the Advanced Photon Source was supported by the U.S. Department of Energy, Office of Science, Office of Basic Energy Sciences, under Contract DE-AC02-06CH11357.

■ REFERENCES

(1) Bethke, C. M.; Sanford, R. A.; Kirk, M. F.; Jin, Q.; Flynn, T. M. The thermodynamic ladder in geomicrobiology. *Am. J. Sci.* **2011**, *311* (3), 183−210.

(2) Postma, D.; Jakobsen, R. Redox zonation: Equilibrium constraints on the Fe(III)/SO_4-reduction interface. *Geochim. Cosmochim. Acta* **1996**, *60* (17), 3169−3175.

(3) Anderson, R.; Vrionis, H.; Ortiz-Bernad, I.; Resch, C.; Long, P.; Dayvault, R.; Karp, K.; Marutzky, S.; Metzler, D.; Peacock, A.; White, D.; Lowe, M.; Lovley, D. Stimulating the in situ activity of Geobacter species to remove uranium from the groundwater of a uranium-contaminated aquifer. *Appl. Environ. Microbiol.* **2003**, 5884−5891.

(4) N'Guessan, A. L.; Vrionis, H. A.; Resch, C. T.; Long, P. E.; Lovley, D. R. Sustained Removal of Uranium From Contaminated Groundwater Following Stimulation of Dissimilatory Metal Reduction. *Environ. Sci. Technol.* **2008**, *42* (8), 2999−3004.

(5) Burkhardt, E.-M.; Akob, D. M.; Bischoff, S.; Sitte, J.; Kostka, J. E.; Banerjee, D.; Scheinost, A. C.; Küsel, K. Impact of Biostimulated Redox Processes on Metal Dynamics in an Iron-Rich Creek Soil of a Former Uranium Mining Area. *Environ. Sci. Technol.* **2009**, *44* (1), 177−183.

(6) Istok, J.; Senko, J.; Krumholz, L.; Watson, D.; Bogle, M.; Peacock, A.; Chang, Y.; White, D. In situ bioreduction of technetium and uranium in a nitrate-contaminated aquifer. *Environ. Sci. Technol.* **2004**, 468−475.

(7) Kappler, A.; Straub, K. L. Geomicrobiological Cycling of Iron. *Rev. Mineral. Geochem.* **2005**, *59* (1), 85−108.

(8) Kostka, J.; Dalton, D.; Skelton, H.; Dollhopf, S.; Stucki, J. Growth of iron(III)-reducing bacteria on clay minerals as the sole electron acceptor and comparison of growth yields on a variety of oxidized iron forms. *Appl. Environ. Microbiol.* **2002**, *68* (12), 6256−62.

(9) Zachara, J.; Kukkadapu, R.; Fredrickson, J.; Gorby, Y.; Smith, S. Biomineralization of poorly crystalline Fe(III) oxides by dissimilatory metal reducing bacteria (DMRB). *Geomicrobiol. J.* **2002**, 179−207.

(10) Wielinga, B.; Bostick, B.; Hansel, C. M.; Rosenzweig, R. F.; Fendorf, S. Inhibition of Bacterially Promoted Uranium Reduction: Ferric (Hydr)oxides as Competitive Electron Acceptors. *Environ. Sci. Technol.* **2000**, *34* (11), 2190−2195.

(11) Finneran, K.; Housewright, M.; Lovley, D. Multiple influences of nitrate on uranium solubility during bioremediation of uranium-contaminated subsurface sediments. *Environ. Microbiol.* **2002**, 510−516.

(12) Liu, C.; Zachara, J. M.; Gorby, Y. A.; Szecsody, J. E.; Brown, C. F. Microbial Reduction of Fe(III) and Sorption/Precipitation of Fe(II) on *Shewanella putrefaciens* Strain CN32. *Environ. Sci. Technol.* **2001**, *35* (7), 1385−1393.

(13) Bell, P. E.; Mills, A. L.; Herman, J. S. Biogeochemical Conditions Favoring Magnetite Formation during Anaerobic Iron Reduction. *Appl. Environ. Microbiol.* **1987**, *53* (11), 2610−2616.

(14) Dong, H.; Fredrickson, J. K.; Kennedy, D. W.; Zachara, J. M.; Kukkadapu, R. K.; Onstott, T. C. Mineral transformations associated with the microbial reduction of magnetite. *Chem. Geol.* **2000**, *169* (3−4), 299−318.

(15) Fredrickson, J. K.; Zachara, J. M.; Kennedy, D. W.; Dong, H.; Onstott, T. C.; Hinman, N. W.; Li, S.-m. Biogenic iron mineralization accompanying the dissimilatory reduction of hydrous ferric oxide by a groundwater bacterium. *Geochim. Cosmochim. Acta* **1998**, *62* (19−20), 3239−3257.

(16) O'Loughlin, E.; Larese-Casanova, P.; Scherer, M.; Cook, R. Green rust formation from the bioreduction of gamma-FeOOH

(lepidocrocite): Comparison of several Shewanella species. *Geomicrobiol. J.* **2007**, 211−230.
(17) O'Loughlin, E. J.; Kelly, S. D.; Kemner, K. M. XAFS Investigation of the Interactions of UVI with Secondary Mineralization Products from the Bioreduction of FeIII Oxides. *Environ. Sci. Technol.* **2010**, *44* (5), 1656−1661.
(18) Komlos, J.; Moon, H.; Jaffe, P. Effect of Sulfate on the Simultaneous Bioreduction of Iron and Uranium. *J. Environ. Qual.* **2008**, 2058−2062.
(19) Roden, E. E.; Zachara, J. M. Microbial Reduction of Crystalline Iron(III) Oxides: Influence of Oxide Surface Area and Potential for Cell Growth. *Environ. Sci. Technol.* **1996**, *30* (5), 1618−1628.
(20) Zachara, J. M.; Fredrickson, J. K.; Li, S. M.; Kennedy, D. W.; Smith, S. C.; Gassman, P. L. Bacterial reduction of crystalline Fe^{3+} oxides in single phase suspensions and subsurface materials. *Am. Mineral.* **1998**, *83* (11-12, Part 2), 1426−1443.
(21) Roh, Y.; Zhang, C.-L.; Vali, H.; Lauf, R. J.; Zhou, J.; Phelps, T. J. Biogeochemical and environmental factors in Fe biomineralization: Magnetite and siderite formation. *Clays Clay Miner.* **2003**, *51* (1), 83−95.
(22) Veeramani, H.; Alessi, D. S.; Suvorova, E. I.; Lezama-Pacheco, J. S.; Stubbs, J. E.; Sharp, J. O.; Dippon, U.; Kappler, A.; Bargar, J. R.; Bernier-Latmani, R. Products of abiotic U(VI) reduction by biogenic magnetite and vivianite. *Geochim. Cosmochim. Acta* **2011**, *75* (9), 2512−2528.
(23) Behrends, T.; Van Cappellen, P. Competition between enzymatic and abiotic reduction of uranium(VI) under iron reducing conditions. *Chem. Geol.* **2005**, *220* (3−4), 315−327.
(24) Fredrickson, J.; Zachara, J.; Kennedy, D.; Duff, M.; Gorby, Y.; Li, S.; Krupka, K. Reduction of U(VI) in goethite (alpha-FeOOH) suspensions by a dissimilatory metal-reducing bacterium. *Geochim. Cosmochim. Acta* **2000**, 3085−3098.
(25) Charlet, L.; Liger, E.; Gerasimo, P. Decontamination of TCE- and U-Rich Waters by Granular Iron: Role of Sorbed Fe(II). *J. Environ. Eng.* **1998**, *124* (1), 25−30.
(26) Jeon, B.-H.; Kelly, S. D.; Kemner, K. M.; Barnett, M. O.; Burgos, W. D.; Dempsey, B. A.; Roden, E. E. Microbial Reduction of U(VI) at the Solid−Water Interface. *Environ. Sci. Technol.* **2004**, *38* (21), 5649−5655.
(27) Liger, E.; Charlet, L.; Van Cappellen, P. Surface catalysis of uranium(VI) reduction by iron(II). *Geochim. Cosmochim. Acta* **1999**, *63* (19−20), 2939−2955.
(28) Regenspurg, S.; Schild, D.; Schäfer, T.; Huber, F.; Malmström, M. E. Removal of uranium(VI) from the aqueous phase by iron(II) minerals in presence of bicarbonate. *Appl. Geochem.* **2009**, *24* (9), 1617−1625.
(29) Chakraborty, S.; Favre, F.; Banerjee, D.; Scheinost, A. C.; Mullet, M.; Ehrhardt, J.-J.; Brendle, J.; Vidal, L. c.; Charlet, L. U(VI) Sorption and Reduction by Fe(II) Sorbed on Montmorillonite. *Environ. Sci. Technol.* **2010**, *44* (10), 3779−3785.
(30) Jeon, B.-H.; Dempsey, B. A.; Burgos, W. D.; Barnett, M. O.; Roden, E. E. Chemical Reduction of U(VI) by Fe(II) at the Solid−Water Interface Using Natural and Synthetic Fe(III) Oxides. *Environ. Sci. Technol.* **2005**, *39* (15), 5642−5649.
(31) Boyanov, M. I.; O'Loughlin, E. J.; Roden, E. E.; Fein, J. B.; Kemner, K. M. Adsorption of Fe(II) and U(VI) to carboxyl-functionalized microspheres: The influence of speciation on uranyl reduction studied by titration and XAFS. *Geochim. Cosmochim. Acta* **2007**, *71* (8), 1898−1912.
(32) O'Loughlin, E.; Kelly, S.; Cook, R.; Csencsits, R.; Kemner, K. Reduction of Uranium(VI) by mixed iron(II/iron(III) hydroxide (green rust): Formation of UO_2 manoparticles. *Environ. Sci. Technol.* **2003**, 721−727.
(33) Ilton, E. S.; Haiduc, A.; Moses, C. O.; Heald, S. M.; Elbert, D. C.; Veblen, D. R. Heterogeneous reduction of uranyl by micas: Crystal chemical and solution controls. *Geochim. Cosmochim. Acta* **2004**, *68* (11), 2417−2435.
(34) Ilton, E. S.; Heald, S. M.; Smith, S. C.; Elbert, D.; Liu, C. Reduction of Uranyl in the Interlayer Region of Low Iron Micas under Anoxic and Aerobic Conditions. *Environ. Sci. Technol.* **2006**, *40* (16), 5003−5009.
(35) Wersin, P.; Hochella, M. F., Jr.; Persson, P.; Redden, G.; Leckie, J. O.; Harris, D. W. Interaction between aqueous uranium (VI) and sulfide minerals: Spectroscopic evidence for sorption and reduction. *Geochim. Cosmochim. Acta* **1994**, *58* (13), 2829−2843.
(36) Bruggeman, C.; Maes, N. Uptake of Uranium(VI) by Pyrite under Boom Clay Conditions: Influence of Dissolved Organic Carbon. *Environ. Sci. Technol.* **2010**, *44* (11), 4210−4216.
(37) Qafoku, N. P.; Kukkadapu, R. K.; McKinley, J. P.; Arey, B. W.; Kelly, S. D.; Wang, C.; Resch, C. T.; Long, P. E. Uranium in Framboidal Pyrite from a Naturally Bioreduced Alluvial Sediment. *Environ. Sci. Technol.* **2009**, *43* (22), 8528−8534.
(38) Hyun, S. P.; Davis, J. A.; Sun, K.; Hayes, K. F. Uranium(VI) Reduction by Iron(II) Monosulfide Mackinawite. *Environ. Sci. Technol.* **2012**, *46* (6), 3369−3376.
(39) Moyes, L. N.; Parkman, R. H.; Charnock, J. M.; Vaughan, D. J.; Livens, F. R.; Hughes, C. R.; Braithwaite, A. Uranium Uptake from Aqueous Solution by Interaction with Goethite, Lepidocrocite, Muscovite, and Mackinawite: An X-ray Absorption Spectroscopy Study. *Environ. Sci. Technol.* **2000**, *34* (6), 1062−1068.
(40) Livens, F. R.; Jones, M. J.; Hynes, A. J.; Charnock, J. M.; Mosselmans, J. F. W.; Hennig, C.; Steele, H.; Collison, D.; Vaughan, D. J.; Pattrick, R. A. D.; Reed, W. A.; Moyes, L. N. X-ray absorption spectroscopy studies of reactions of technetium, uranium and neptunium with mackinawite. *J. Environ. Radioact.* **2004**, *74* (1−3), 211−219.
(41) Hua, B.; Deng, B. Reductive Immobilization of Uranium(VI) by Amorphous Iron Sulfide. *Environ. Sci. Technol.* **2008**, *42* (23), 8703−8708.
(42) Abdelouas, A.; Lutze, W.; Nuttall, H. E. Oxidative dissolution of uraninite precipitated on Navajo sandstone. *J. Contam. Hydrol.* **1999**, *36* (3−4), 353−375.
(43) Personna, Y. R.; Ntarlagiannis, D.; Slater, L.; Yee, N.; O'Brien, M.; Hubbard, S. Spectral induced polarization and electrodic potential monitoring of microbially mediated iron sulfide transformations. *J. Geophys. Res.* **2008**, *113* (G2), G02020.
(44) Williams, K. H.; Ntarlagiannis, D.; Slater, L. D.; Dohnalkova, A.; Hubbard, S. S.; Banfield, J. F. Geophysical Imaging of Stimulated Microbial Biomineralization. *Environ. Sci. Technol.* **2005**, *39* (19), 7592−7600.
(45) Williams, K. H.; Kemna, A.; Wilkins, M. J.; Druhan, J.; Arntzen, E.; N'Guessan, A. L.; Long, P. E.; Hubbard, S. S.; Banfield, J. F. Geophysical Monitoring of Coupled Microbial and Geochemical Processes During Stimulated Subsurface Bioremediation. *Environ. Sci. Technol.* **2009**, *43* (17), 6717−6723.
(46) Butler, I. B.; Rickard, D. Framboidal pyrite formation via the oxidation of iron (II) monosulfide by hydrogen sulphide. *Geochim. Cosmochim. Acta* **2000**, *64* (15), 2665−2672.
(47) Sweeney, R. E.; Kaplan, I. R. Pyrite Framboid Formation; Laboratory Synthesis and Marine Sediments. *Econ. Geol.* **1973**, *68* (5), 618−634.
(48) Berner, R. A. Sedimentary pyrite formation. *Am. J. Sci.* **1970**, *268* (1), 1−23.
(49) Patterson, R. R.; Fendorf, S.; Fendorf, M. Reduction of Hexavalent Chromium by Amorphous Iron Sulfide. *Environ. Sci. Technol.* **1997**, *31* (7), 2039−2044.
(50) Scheinost, A. C.; Charlet, L. Selenite Reduction by Mackinawite, Magnetite and Siderite: XAS Characterization of Nanosized Redox Products. *Environ. Sci. Technol.* **2008**, *42* (6), 1984−1989.
(51) Stookey, L. L. Ferrozine—A new spectrophotometric reagent for iron. *Anal. Chem.* **1970**, *42* (7), 779−781.
(52) Integrated X-ray powder diffraction software. *Rigaku J.* **2010**, *26*, (1), 23−27.
(53) Peretyazhko, T. S.; Zachara, J. M.; Kukkadapu, R. K.; Heald, S. M.; Kutnyakov, I. V.; Resch, C. T.; Arey, B. W.; Wang, C. M.; Kovarik, L.; Phillips, J. L.; Moore, D. A. Pertechnetate (TcO4−) reduction by reactive ferrous iron forms in naturally anoxic, redox transition zone

sediments from the Hanford Site, USA. *Geochim. Cosmochim. Acta* **2012**, *92* (0), 48−66.
(54) Rancourt, D. G.; Ping, J. Y. Voigt-based methods for arbitrary-shape static hyperfine parameter distributions in Mössbauer spectroscopy. *Nucl. Instrum. Methods Phys. Res., Sect. B* **1991**, *58* (1), 85−97.
(55) Ressler, T. WinXAS: a program for X-ray absorption spectroscopy data analysis under MS-Windows. *J Synchrotron Radiat.* **1998**, *5*, 118−122.
(56) Hunger, S.; Benning, L. Greigite: A true intermediate on the polysulfide pathway to pyrite. *Geochem. Trans.* **2007**, *8* (1), 1.
(57) Herbert, R. B., Jr.; Benner, S. G.; Pratt, A. R.; Blowes, D. W. Surface chemistry and morphology of poorly crystalline iron sulfides precipitated in media containing sulfate-reducing bacteria. *Chem. Geol.* **1998**, *144* (1−2), 87−97.
(58) Mullet, M.; Boursiquot, S.; Abdelmoula, M.; Genin, J. M.; Ehrhardt, J. J. Surface chemistry and structural properties of mackinawite prepared by reaction of sulfide ions with metallic iron. *Geochim. Cosmochim. Acta* **2002**, *66* (5), 829−836.
(59) Ohfuji, H.; Rickard, D. High resolution transmission electron microscopic study of synthetic nanocrystalline mackinawite. *Earth Planet. Sci. Lett.* **2006**, *241* (1−2), 227−233.
(60) Jeong, H. Y. Characterization of synthetic nanocrystalline mackinawite: Crystal structure, particle size, and specific surface area. *Geochim. Cosmochim. Acta* **2008**, *72* (2), 493−505.
(61) Murad, E.; Cashion, J. *Mössbauer Spectroscopy of Environmental Materials and Their Industrial Utilization*; Kluwer Academic Publishers: Boston, MA, 2004.
(62) Mycroft, J. R.; Bancroft, G. M.; McIntyre, N. S.; Lorimer, J. W.; Hill, I. R. Detection of sulphur and polysulphides on electrochemically oxidized pyrite surfaces by X-ray photoelectron spectroscopy and Raman spectroscopy. *J. Electroanal. Chem. Interfacial Electrochem.* **1990**, *292* (1−2), 139−152.
(63) Nesbitt, H. W.; Bancroft, G. M.; Pratt, A. R.; Scaini, M. J. Sulfur and iron surface states on fractured pyrite surfaces. *Am. Mineral.* **1998**, *83* (9−10), 1067−1076.
(64) Alessi, D. S.; Uster, B.; Veeramani, H.; Suvorova, E. I.; Lezama-Pacheco, J. S.; Stubbs, J. E.; Bargar, J. R.; Bernier-Latmani, R. Quantitative Separation of Monomeric U(IV) from UO_2 in Products of U(VI) Reduction. *Environ. Sci. Technol.* **2012**, *46* (11), 6150−6157.
(65) Pratt, A. R.; Muir, I. J.; Nesbitt, H. W. X-ray photoelectron and Auger electron spectroscopic studies of pyrrhotite and mechanism of air oxidation. *Geochim. Cosmochim. Acta* **1994**, *58* (2), 827−841.
(66) Jones, C. F.; LeCount, S.; Smart, R. S. C.; White, T. J. Compositional and structural alteration of pyrrhotite surfaces in solution: XPS and XRD studies. *Appl. Surf. Sci.* **1992**, *55* (1), 65−85.
(67) Baltrus, J. P.; Proctor, A. Composition of overlayers on oxidized pyrite surfaces. *Appl. Surf. Sci.* **1990**, *44* (2), 147−150.
(68) Bancroft, G. M.; Hyland, M. M. Spectroscopic studies of adsorption/reduction reactions of aqueous metal complexes on sulphide surfaces. *Rev. Mineral. Geochem.* **1990**, *23* (1), 511−558.
(69) Langmuir, D. Uranium solution-mineral equilibria at low temperatures with applications to sedimentary ore deposits. *Geochim. Cosmochim. Acta* **1978**, *42* (6, Part 1), 547−569.
(70) Lisitsin, A. K. Form of occurrence of uranium in ground waters and conditions of precipitation as UO_2. *Geokhimiya* **1962**, *9*, 763−769.
(71) Lovley, D. R.; Phillips, E. J. P.; Gorby, Y. A.; Landa, E. R. Microbial Reduction of Uranium. *Nature* **1991**, *350* (6317), 413−416.
(72) Dullies, F.; Lutze, W.; Gong, W.; Nuttall, H. E. Biological reduction of uranium—From the laboratory to the field. *Sci. Total Environ.* **2010**, *408* (24), 6260−6271.
(73) Abdelouas, A.; Lu, Y.; Lutze, W.; Nuttall, H. E. Reduction of U(VI) to U(IV) by indigenous bacteria in contaminated ground water. *J. Contam. Hydrol.* **1998**, *35* (1−3), 217−233.
(74) Cardenas, E.; Wu, W.-M.; Leigh, M. B.; Carley, J.; Carroll, S.; Gentry, T.; Luo, J.; Watson, D.; Gu, B.; Ginder-Vogel, M.; Kitanidis, P. K.; Jardine, P. M.; Zhou, J.; Criddle, C. S.; Marsh, T. L.; Tiedje, J. M. Microbial Communities in Contaminated Sediments, Associated with Bioremediation of Uranium to Submicromolar Levels. *Appl. Environ. Microbiol.* **2008**, *74* (12), 3718−3729.
(75) Descostes, M.; Schlegel, M. L.; Eglizaud, N.; Descamps, F.; Miserque, F.; Simoni, E. Uptake of uranium and trace elements in pyrite (FeS_2) suspensions. *Geochim. Cosmochim. Acta* **2010**, *74* (5), 1551−1562.
(76) Rickard, D. T. Kinetics and mechanism of pyrite formation at low temperatures. *Am. J. Sci.* **1975**, *275* (6), 636−652.
(77) Veeramani, H.; Schofield, E. J.; Sharp, J. O.; Suvorova, E. I.; Ulrich, K. U.; Mehta, A.; Giammar, D. E.; Bargar, J. R.; Bernier-Latmanit, R. Effect of Mn(II) on the structure and reactivity of biogenic uraninite. *Environ. Sci. Technol.* **2009**, *43* (17), 6541−7.